Analytica Chimica Acta 1169 (2021) 338628

Contents lists available at ScienceDirect

Analytica Chimica Acta

journal homepage: www.elsevier.com/locate/aca

A novel signal amplification label based on AuPt alloy nanoparticles supported by high-active carbon for the electrochemical detection of circulating tumor DNA

Kaicha Chen [a], Hongli Zhao [a, **], Zhenxing Wang [a], Minbo Lan [a, b, *]

[a] Shanghai Key Laboratory of Functional Materials Chemistry, School of Chemistry and Molecular Engineering, East China University of Science and Technology, Shanghai, 200237, People's Republic of China
[b] Research Center of Analysis and Test, East China University of Science and Technology, Shanghai, 200237, People's Republic of China

HIGHLIGHTS

- A sandwich-type ctDNA electrochemical biosensor was designed based on HAC-AuPt.
- The HAC-AuPt contains high-active sites of N, graphitized-C, Co-Nx, and AuPt alloy.
- The current signal could be amplified largely by the synthesized HAC-AuPt.
- The biosensor exhibits satisfying sensitivity and high selectivity for ctDNA detection.

GRAPHICAL ABSTRACT

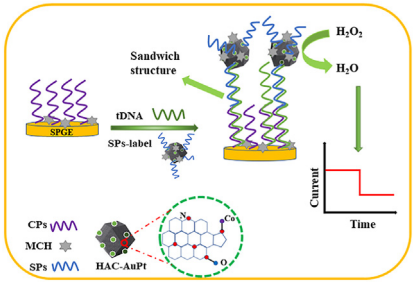

ARTICLE INFO

Article history:
Received 9 March 2021
Received in revised form
27 April 2021
Accepted 6 May 2021
Available online 10 May 2021

Keywords:
Signal amplification
Bimetallic zeolitic imidazolate frameworks
AuPt alloy
Circulating tumor DNA
Sandwich-type electrochemical biosensor

ABSTRACT

The detection of circulating tumor DNA (ctDNA) has increasingly received a great deal of attention considering its significance in cancer diagnosis. And the signal amplification plays an important role in the development of sensitive ctDNA biosensors. Herein, the nanocomposites (denoted as HAC-AuPt), integrating from high-active carbon (HAC) and AuPt alloy nanoparticles, were synthesized and subsequently used as a signal amplification label to fabricate a sandwich-type ctDNA electrochemical biosensor. Characterizations demonstrated that HAC presents uniform size distribution and AuPt alloy nanoparticles were successfully loaded on HAC. The current response could be amplified to a great extent by the resultant HAC-AuPt due to its excellent electrochemical property. The nanocomposites were further bounded with DNA signal probes (SPs) via Au-S or Pt-S assembly to form SPs-label. After the capture probes (CPs) were immobilized on the electrode surface, the target DNA (tDNA) and SPs-label were stepwise incubated on the CPs-modified electrode, thus forming a sandwich-type structure. By monitoring the catalytic signal of HAC-AuPt towards the reduction process of H_2O_2, this biosensor provided a wide linear range of 10^{-8} mol/L - 10^{-16} mol/L with a low detection limit of 3.6×10^{-17} mol/L (S/N = 3) for the detection of the tDNA. Furthermore, obvious differences in response signals among different DNAs were observed benefitting from the excellent selectivity of the biosensor. Besides, the long-term stability, reproducibility, and recovery rate were proved to be outstanding. These results indicate that the established biosensor holds a potential application in the clinical diagnosis of ctDNA.

* Corresponding author. Shanghai Key Laboratory of Functional Materials Chemistry, School of Chemistry and Molecular Engineering, East China University of Science and Technology, Shanghai, 200237, People's Republic of China.
** Corresponding author.
E-mail addresses: honglizhao@ecust.edu.cn (H. Zhao), minbolan@ecust.edu.cn (M. Lan).

https://doi.org/10.1016/j.aca.2021.338628
0003-2670/

1. Introduction

The diagnosis of cancer has become rather important since the deaths resulting from cancer account for a noticeable proportion of the global total death toll [1]. Traditional tissue biopsy has been accepted as a gold standard technology for cancer diagnosis, yet it has some limitations such as time-consuming [2,3]. In contrast, liquid biopsy has not only been proven to be safer and less invasive but also allowed repeated sampling, thereby reducing the suffering of patients, monitoring the evolutionary dynamics of cancer and the risk of treatment [4,5]. Previous researches have proved that circulating tumor DNA (ctDNA), originating from tumors and may carry the same mutations and genetic alterations as those of primary tumors, is one of the particularly informative cancer biomarkers and could potentially serve as a "liquid biopsy" for cancer diagnosis even at early stages, resulting in avoiding conventional tissue biopsy [6]. Moreover, compared with single-site tissue biopsy, the analysis of ctDNA may provide a relatively comprehensive snapshot of intra-tumor clonal heterogeneity for the reason that ctDNA stems from multiple tumor sites [7].

In the past decades, many methods have been developed for the sensing of ctDNA such as PCR [8], DNA sequencing [9], surface-enhanced Raman scattering [10], and electrochemical methods [11]. Among these technologies, electrochemical biosensors have attracted extensive interest because of their advantages of low cost, easy operation, quick response, and time-saving [12–14]. However, the sensitive analysis of ctDNA in biological samples remains a challenging task resulting from the small current response on account of the low concentration of ctDNA (<1% in many cases, sometimes < 0.01%) and the co-existence of different kinds of mutated DNA sequences as interferences [9,15]. Therefore, it is rather urgent to amplify the current response signal for improving the sensitivity of ctDNA electrochemical biosensors. Recently, a sensitive electrochemical immunosensor based on the novel signal amplification system of AuPdCu ternary nanoparticles functionalized polymer nanospheres was designed for the quantitative detection of hepatitis B surface antigen [16]. Similar immunosensors using various nanomaterials as labels for signal amplification have been widely established by other researchers and also showed fascinating performance [17,18]. Inspired by these, it is assumpted that the sandwich-type scheme for antigen detection may be suitable for ctDNA analysis as well.

A well-designed nanomaterial as a label is the key to amplify the current signal, therefore improving the performance of electrochemical sensors [19]. Among the many synthesized nanomaterials, precious metal nanoparticles such as gold (Au) and platinum (Pt) nanoparticles are widely used to catalyze electroactive molecules to enhance current response due to their excellent conductivity and high catalytic capacity [20,21]. Moreover, Au and Pt could bond up with thiol-modified signal probes (SPs) to easily form SPs-label [22,23]. Multi-metallic or alloy nanoparticles could further exhibit better performance due to the multifunctional or synergistic effects [24–26]. However, nanoparticles would suffer from severe aggregation without the assistance of support, causing waste and a decrease in their intrinsic catalytic property [27]. The utilization of the zeolitic imidazolate frameworks (ZIFs) as support has been proved to be a good solution to address this hurdle due to its easy preparation as well as the large area provided by its polyhedral morphology [28]. Moreover, ZIFs have been identified as precursors for the preparation of carbon catalysts as they are rich in carbon, nitrogen, and transition metals [29]. Carbon nanomaterials derived from the carbonization of ZIFs exhibit a more satisfying catalytic and conductive ability [30]. Especially high-active carbon (HAC), deriving from ZIF-8 and ZIF-67, has been demonstrated to be one of the most fascinating catalysts for oxygen reduction reaction and other electrochemical sensing processes [31,32]. The HAC not only possesses a small size and high nitrogen content of ZIF-8 but has good graphitized carbon and high catalytic cobalt species of ZIF-67 as well [29,33], thus rendering the carbon nanomaterial high-active sites of N, good graphitized carbon, and Co-Nx for electrocatalysis.

In this work, the HAC-AuPt nanocomposites were synthesized and used as a label for signal amplification to establish a novel sandwich-type biosensor for the electrochemical analysis of ctDNA. The HAC-AuPt was prepared through simple annealing of bimetallic ZIFs precursor and an in-situ reduction process of AuPt mixture solution. Both the HAC and AuPt alloy nanoparticles (AuPtNPs) show satisfying electrochemical performance. The combination of HAC and AuPt alloy further improves the current response and provides sufficient sites for immobilizing SPs, while preventing the aggregation of nanoparticles. As a result, the proposed biosensor based on HAC-AuPt exhibits high performance in ctDNA detection.

2. Experimental

2.1. Chemicals and apparatus

$K_3[Fe(CN)_6]$, $K_4[Fe(CN)_6]$, H_2O_2 (30%), $H_2PtCl_6 \cdot 6H_2O$, $HAuCl_4 \cdot 4H_2O$, NaCl, KCl, $NaBH_4$ were purchased from Sinopharm Chemical Reagent Co., Ltd. Polyvinylpyrrolidone (PVP), 2-methylimidazole, tris(hydroxymethyl)methyl aminomethane (Tris), $Co(NO_3)_2 \cdot 6H_2O$, $Zn(NO_3)_2 \cdot 6H_2O$, tri(2-chloroethyl) phosphate (TCEP), HCl, 6-mercapto-1-hexanol (MCH) were bought from Aladdin Industrial Inc. KH_2PO_4, Na_2HPO_4 were pursued from Shanghai Lingfeng Chemical Reagent Co., Ltd. Phosphate buffer saline (PBS, pH = 7.5) was made of KH_2PO_4, Na_2HPO_4, and KCl. Tris-HCl (TH, pH = 7.5) buffer consisted of Tris, HCl, and NaCl. All the chemicals were used directly as received without any further purification. The ultrapure water used in the whole experiment was homemade by a Laboratory Water Purification System (18.2 M cm). Healthy human serum samples were provided by volunteers from our laboratory.

Transmission electron microscopy (TEM) and scanning electron microscopy (SEM) images were obtained from a JEM-1400 TEM (JEOL, Japan) and an S-3400 N SEM (Hitachi, Japan), respectively. The energy dispersive spectrum (EDS) and elemental mapping patterns were investigated using an XM-2 energy dispersive spectrometer equipped with a Tecnai G2 F30 S-TWIN field emission TEM (FEI, USA). Zeta potential measurements were carried out on a Nano-ZS90 instrument (Malvern, UK). The XPS analysis was performed on an ESCALAB 250Xi X-ray photoelectron spectrometer (Thermo Fisher, USA) and all the reported binding energy data was calibrated using C 1s (284.8 eV). The X-ray diffraction (XRD) patterns of samples were recorded using a D/MAX2550 diffractometer (Rigaku International Co., Japan).

The DNA oligonucleotides related to breast cancer used in the experiment were synthesized and purified by Shanghai Sangon Biotech Co., Ltd. and their sequence information is listed in Table S1 (Supplementary material).

2.2. Preparation of HAC-AuPt nanocomposites

HAC was synthesized according to the literature [29] with some modification. 1.60 g $Zn(NO_3)_2 \cdot 6H_2O$ and 0.078 g $Co(NO_3)_2 \cdot 6H_2O$ were dissolved in 80 mL methanol under sonication until a transparent solution was obtained. Then, 80 mL methanol containing 3.70 g 2-methylimidazole was poured into the above solution and stirred for 24 h. The as-obtained purple product (denoted as

BMZIFs) was centrifuged and washed with methanol several times. After drying in a 60 °C vacuum oven, the BMZIFs powders were placed in a tube furnace and calcined at 900 °C for 2 h with a heating rate of 5 °C/min under flowing N_2 gas and then cooled naturally to obtain HAC. To synthesize HAC-AuPt, 0.01 g PVP and 20 mg HAC were dispersed in 45 mL water under ultrasonication. Then, 25.8 mg $H_2PtCl_6 \cdot 6H_2O$ and 1.7 mg $HAuCl_4 \cdot 4H_2O$ were added under stirring followed by dropping 5 mL $NaBH_4$ (6 mg/mL) and stirred for another 4 h. The product was collected by centrifugation followed by washed with ethanol and water three times. For comparison, AuPtNPs, HAC-Au, and HAC-Pt were synthesized using the identical procedure without HAC as support and without adding $HAuCl_4 \cdot 4H_2O$ or $H_2PtCl_6 \cdot 6H_2O$.

2.3. Fabrication of biosensor based on HAC-AuPt nanocomposites

Screen-printed gold electrodes (SPGEs) used in this work were homemade and were further used to fabricate ctDNA biosensors. Firstly, 20 μL TH buffer containing capture probes (CPs, 10^{-6} mol/L) was dripped on SPGE and stored in a refrigerator at 4 °C overnight for Au-S bond self-assembly [34]. Next, the above CPs/SPGE was further incubated with 20 μL MCH (5 mmol/L) to occupy the nonspecific blank sites. After that, 20 μL target DNA (tDNA) with different concentrations was dropped onto the MCH/CPs/SPGE and incubated for 80 min. Finally, 20 μL mixture solution (termed as SPs-label) containing signal probes (SPs, 10^{-6} mol/L) and HAC-AuPt (2 mg/mL) was dropped onto the tDNA/MCH/CPs/SPGE and incubated for another 70 min. After each step, the modified electrode was washed with water and TH several times to remove unbounded attachments. The biosensors for the detection of base-mismatched DNA sequences were also fabricated through the same process.

2.4. Electrochemical measurements

All amperometric i-t measurements were carried out on a CHI 660D electrochemical workstation (CH Instruments Inc., China) equipped with a traditional three-electrode system consisting of a modified working electrode prepared in each step, a platinum counter electrode, and a reference Ag/AgCl electrode. The I-t tests at a potential of −0.4 V potential were conducted by adding H_2O_2 to PBS buffer under gentle stirring. Cyclic voltammetry (CV) and electrochemical impedance spectroscopy (EIS) measurements were performed on an Autolab M204 electrochemical system (Metrohm, Netherlands). The CV voltage range was set from −0.2 V to 0.6 V with a sweep speed of 0.05 V/s and the EIS measurements were carried out with the frequency ranging from 100 kHz to 0.01 Hz, a voltage of 0.27 V, and an amplitude of 5 mV.

3. Results and discussion

3.1. Preparations and characterizations

The synthesis procedure of HAC-AuPt is illustrated in Scheme 1A. BMZIFs were synthesized by using Zn^{2+} and Co^{2+} as metal sources and 2-methylimidazole as the organic ligand. The as-prepared BMZIFs were calcined at a high temperature to obtain HAC. AuPt alloy nanoparticles were further loaded on HAC via a facile in-situ reduction reaction using $NaBH_4$ as a reducing reagent. The resultant HAC-AuPt was later used as a label to fabricate the sandwich-type ctDNA electrochemical biosensor, as displayed in Scheme 1B. Briefly, CPs modified with -SH were fixed on SPGE via Au-S bond followed by immobilizing MCH to avoid non-specific sites. Subsequently, tDNA was captured by CPs through hybridization reaction and SPs-label was further hybridized with tDNA. Through the stepwise hybridization of CPs, tDNA, and SPs-label, a sandwich structure was formed. Finally, the recognition could be detected by monitoring the reduction of H_2O_2.

The morphologies of the synthesized nanocomposites were visualized by TEM, SEM, and HRTEM. As shown in Fig. 1A, the AuPtNPs without HAC showed small sphere-shaped with a diameter of about 10 nm but suffered from severe aggregation, which could cause adverse influence on its catalytic property [19]. As shown in Fig. 1B and Fig. S1A, the homogeneous polyhedral shapes with a diameter of approximately 100 nm of the well-dispersed BMZIFs. The original morphology of BMZIFs was inherited after the annealing process (Fig. 1C and Fig. S1B), however, its surface became rough could be ascribed to organic ligands was carbonized at high temperature and metal ions transformed into nanoparticles or metal oxides. Comparing with AuPtNPs alone, nanoparticles were uniformly distributed on the HAC surface (Fig. 1D), demonstrating the HAC could act as support to avoid aggregation of AuPt nanoparticles. As shown in the HRTEM image at larger magnification (Fig. 1E), a lot of measured typical lattice spacings of the (111) plane with a width of 0.231 nm were observed, which are smaller than face-centered cubic Pt(111) of 0.226 nm and larger than face-centered cubic Au(111) of 0.235 nm, confirming the formation of AuPt alloy [35] and the HAC-AuPt nanocomposites were prepared successfully. The selected area electron diffraction (SAED) pattern presents several concentric circles that could be ascribed to (111) and (200) planes of AuPt alloy [33] (Fig. 1F), which implies the nanocomposites are polycrystal [36]. To investigate the chemical composition and elemental distribution of the nanocomposites, elemental mapping was applied using EDS in high-angle annular dark-field scanning transmission electron microscopy (HAADF-STEM) mode. As shown in Fig. 1G that HAC-AuPt composites consisted of C, N, Co, Au, and Pt with uniform distribution. Moreover, several peaks of C, N, O, Co, Au, Pt were observed in the EDS spectrum (Fig. S2A). These results further indicate the formation of HAC-AuPt.

To further investigate the crystal structure, powder XRD analysis was conducted and the results are displayed in Fig. S2B. The corresponding XRD patterns for both HAC and HAC-AuPt exhibited a wide peak at around 26°indexed to (002) diffraction of graphite carbon. The peak located at around 44°is assignable to the (111) diffraction of face-centered cubic Co embedded in carbon [29]. After the loading of AuPt, new diffraction peaks centered at 38.3°and 39.9°appeared, which corresponds to (111) plane of face-centered cubic of Au and Pt [33]. Compared with metal Au (JCPDS 01-1172) and Pt (JCPDS 01-1190) [37], there were no peaks of single metal that existed. Moreover, these peaks of HAC-AuPt were slightly shifted to a high 2Θ value compared with commercial Pt/C (JCPDS 04-0601) [26] further demonstrated the formation of an alloy [38].

Besides, XPS characterization was employed to reveal the electronic states and composition of the nanocomposites. The survey spectra of the HAC-AuPt, shown in Fig. 2A, exhibited corresponding reflections of C, N, O, Au, Pt, and Co, which is consistent with the EDS results. The curve resulted in four characteristic reflections at 71.5 eV and 74.5 eV (Fig. 2B) are assignable to Pt4f while 84.1 eV and 87.8 eV are assigned as Au4f, indicating the co-existence of Pt and Au. Compared to the standard value of XPS energy of Pt, the peak of Pt4f in this work exhibited a negative shift. This is because the electron-interaction of alloy can change the d-band structure of Pt, which is important for catalyst performance and stability [38,39]. The high-resolution XPS spectra for Co 2p in HAC-AuPt (Fig. 2C) showed three types of cobalt species: Co, CoOx (or CoCxNy) as well as Co−Nx. The Co−Nx has been identified as one of the most important active sites in many catalytic processes [29]. The high-resolution N1s spectrum (Fig. 2D) presented five types of N

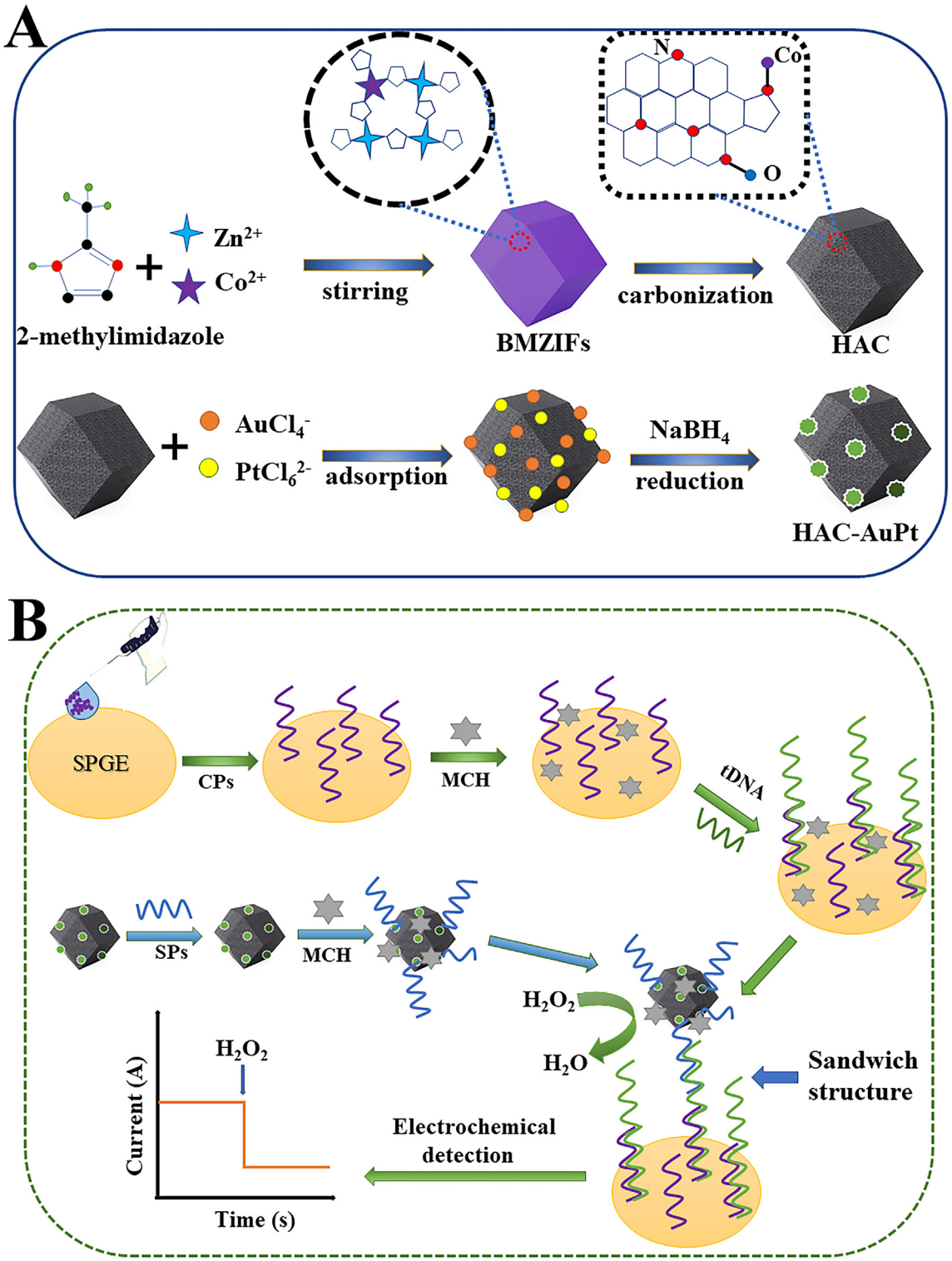

Scheme 1. Schematic illustrations of **(A)** Synthetic steps of HAC-AuPt nanocomposites and **(B)** Fabrication process of sandwich-type ctDNA electrochemical biosensor.

species: pyrrolic-N, oxide-N, pyridine-N, Co-N, and graphitic-N. It has been reported that all these N species play an important role in catalysis except the oxide-N [29]. Pyridine-N has been commonly used to characterize the number of active sites and the graphic-N content has a relationship with the conductivity [40]. The high content of these two types of N species indicated the satisfactory active sites and good conductivity of HAC-AuPt, which was further confirmed by electrochemical tests in the later section.

3.2. Characterizations of electrochemical performance with different nanomaterials

To verify the significance of HAC-AuPt for signal amplification, the electrochemical performance of different nanomaterials

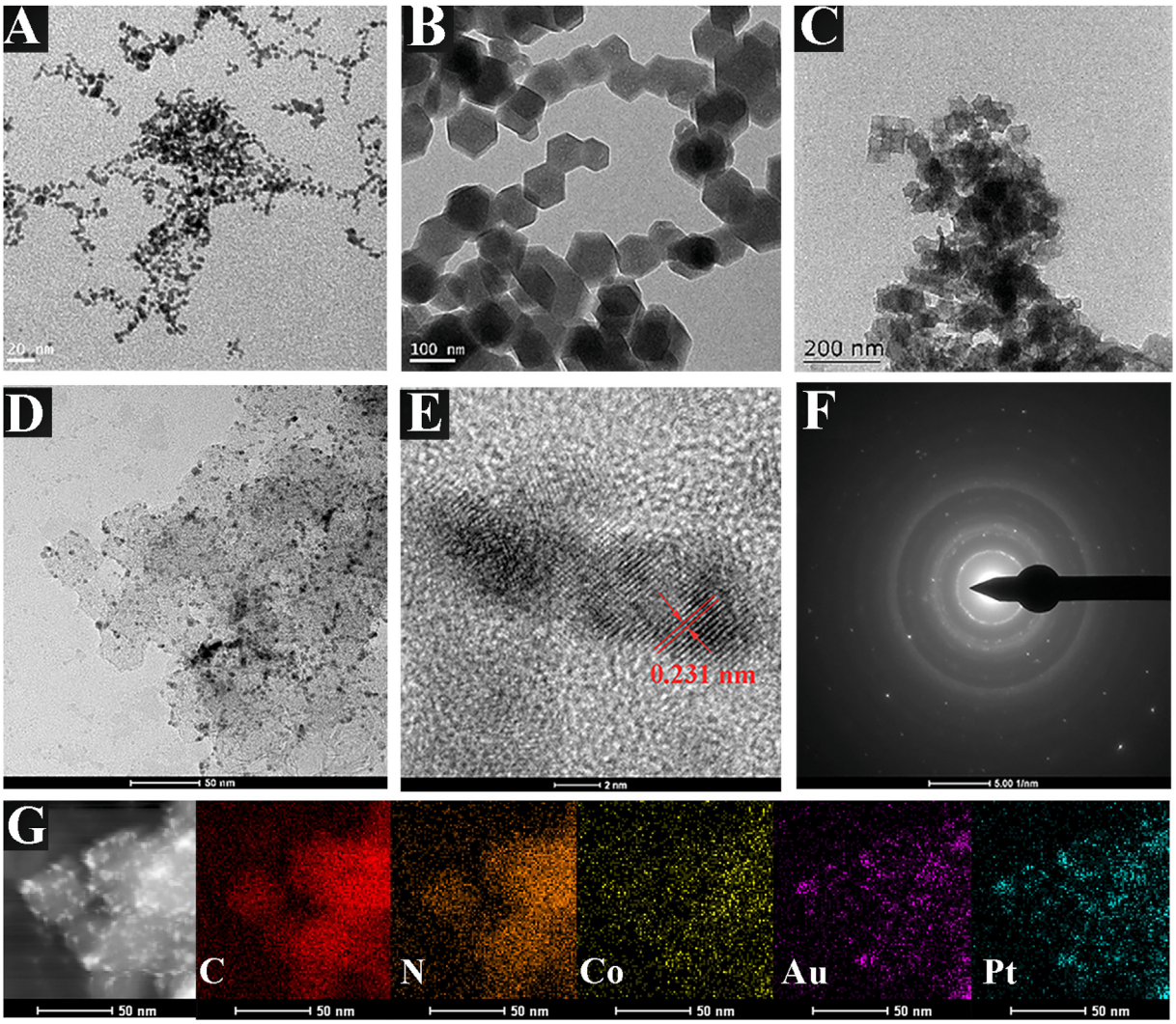

Fig. 1. TEM images of **(A)** AuPtNPs **(B)** BMZIFs and **(C)** HAC. **(D)** and **(E)** HRTEM images of HAC-AuPt at two different magnifications. **(F)** SAED pattern and **(G)** HAADF-STEM image and elemental mapping of HAC-AuPt.

prepared in the synthesis process was compared by I-t and CV methods. The bare SPGE (Figs. S3A and S3B, curve a) exhibited a small response towards H_2O_2 because it consists of a layer of dense gold film with a small deficiency which limits its catalytic capacity. The signal of BMZIFs/SPGE (b) was further reduced, which could ascribe to the fact that the organic ligand is insulating. The improved catalytic response of HAC (c) was observed, benefiting from the annealing process. Besides, the synthesized AuPtNPs (d) showed satisfactory response due to the inherent catalytic ability of noble metals. Compared with the above-mentioned nanomaterials, HAC-AuPt (e) displayed the best performance, which could be inferred to arise from the combined effect of Co−Nx species, N species, uniform dispersion of N and Co [29,31], and the synergistic effects of alloy nanoparticles. As shown in Fig. S4, the capacity of HAC-Au and HAC-Pt was worse than HAC-AuPt, further highlighting the advantages of using AuPt alloy [25,41]. To further verify the feasibility of using HAC-AuPt to catalyze H_2O_2, CV responses before and after the addition of H_2O_2 were recorded and the results are shown in Fig. S3C. The signal increased obviously after H_2O_2 was added, proving that HAC-AuPt can be used as a label for signal amplification. Also, the good conductivity of HAC-AuPt (Fig. S3D) reflects the contribution from its graphitization [29]. All these results indicate the excellent electrochemical performance of the synthesized nanocomposites HAC-AuPt.

3.3. Signal recognition of DNA immobilization and hybridization

To investigate whether the different DNA sequences can hybridize with each other and study the electrochemical behavior of different modified electrodes, CV and EIS measurements were performed in a mixture solution composing of 5 mmol/L $[Fe(CN)_6]^{3-/4-}$ and 0.1 mol/L KCl. CV and EIS are effective and convenient methods to probe the interface characteristic of the electrode. The peak current of CV and the semicircle portion of an EIS curve represent the electron transfer resistance while the linear portion of EIS is associated with diffusion [42]. As shown in Fig. 3, the SPGE (curve a) exhibited a pair of very strong peaks which were belonged to the reduction of Fe^{3+} and oxidization of Fe^{2+} [43]. And the corresponding EIS diagram showed the smallest semicircle, demonstrating the good conductivity of SPGE. The resistances of CPs/SPGE (b) and MCH/CPs/SPGE (c) increased stepwise, verifying CPs and MCH were successfully fixed on SPGE via Au-S bond [23]. This can be ascribed to the fact that single-stranded DNA is flexible which can lie down on the electrode surface and the negative charge of its phosphate skeleton [44]. Besides, MCH is insulating, both of which hurdle the $[Fe(CN)_6]^{3-/4-}$ to approach electrode. After

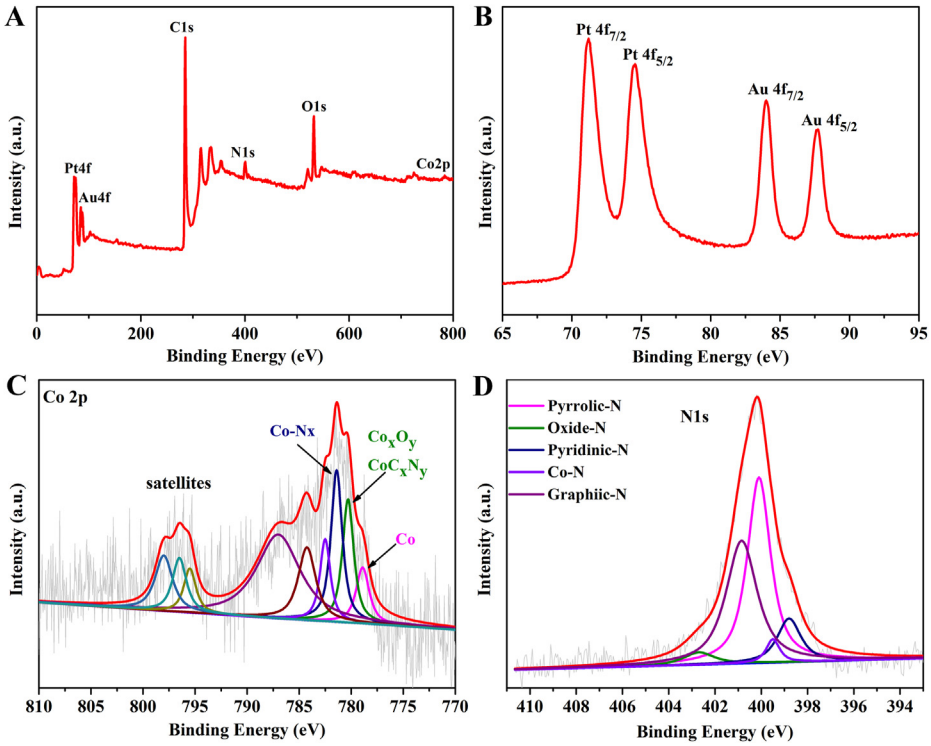

Fig. 2. **(A)** XPS survey spectra of HAC-AuPt. **(B)** Au4f and Pt4f, **(C)** Co2p and **(D)** N1s high-resolution spectra of HAC-AuPt.

the above electrode was immersed in tDNA (d) and then in SPs (e), a gradual increase of resistances was observed, indicating the successful hybridizations of CPs and tDNA, tDNA and SPs. However, the resistance decreased apparently when SPs-label (f) was incubated with tDNA because of the excellent conductivity of HAC-AuPt. Further, the results of the zeta test (Fig. S5) showed a positive charge of the HAC-AuPt, yet it turned negative when SPs were added, which indicates the successful preparation of SPs-label. These results demonstrate that the sandwich-type electrochemical DNA biosensor was fabricated successfully. Besides, the binding constant between the probe and target is calculated to be 1.05×10^8 M^{-1} based on the Scatchard analysis [45] using fluorescence spectra, as shown in Fig. S6.

3.4. Optimization of experiment conditions

To obtain a better analytical performance of this biosensor towards tDNA, several experimental parameters containing pH of the PBS solution, the concentration of HAC-AuPt, and hybridization time were respectively optimized using 10^{-6} mol/L tDNA.

The pH of the PBS has a significant influence on the current response, as shown in Fig. S7A that the signal stepwise increased and then decreased as the pH value continuously increased, and the signal reached the maximum when the pH was set to be 7.5. Therefore, PBS of pH = 7.5 was selected as a suitable value in the whole experiment. As shown in Fig. S7B, the current signal enhanced with the increase of nanocomposites, then decreased after reaching 2 mg/mL. Under the low concentration range of the label, the more the label was used, the more H_2O_2 can be reduced, however, too much nanomaterial can hinder electron transfer [19]. Therefore, HAC-AuPt of 2 mg/mL was used in the experiment. Further, to save operation time, the hybridization times were optimized and the results are presented in Figs. S7C and D. There was no increase of the current signal any longer when the

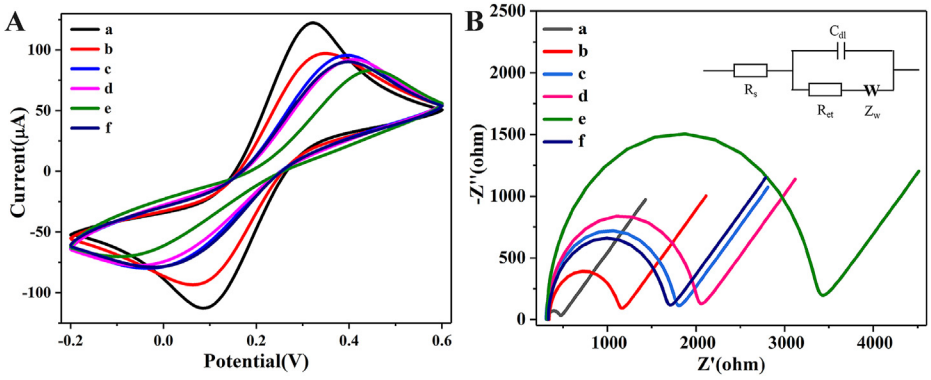

Fig. 3. **(A)** CV and Nyquist plots **(B)** of stepwise-modified electrodes: (a) SPGE, (b) CPs/SPG E, (c) MCH/CPs/SPGE, (d) tDNA/MCH/CPs/SPGE, (e) SPs/tDNA/MCH/CPs/SPGE, and (f) SPs-label/tDNA/MCH/CPs/SPGE.

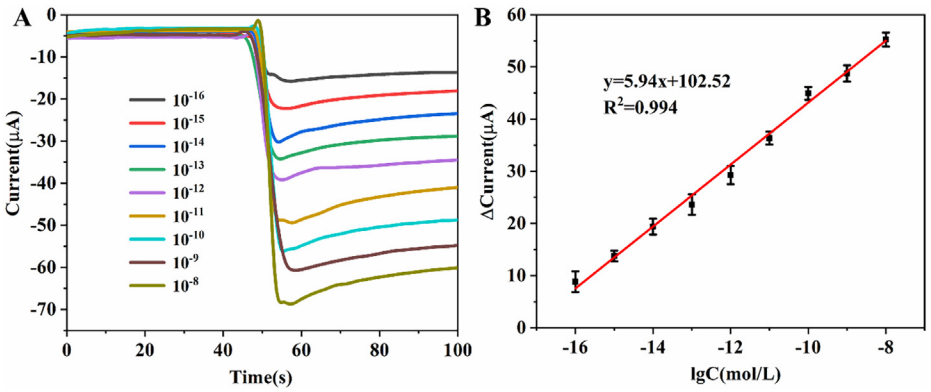

Fig. 4. **(A)** Amperometric i-t curves and **(B)** Calibration curve of the biosensor towards different concentrations of tDNA.

incubation time of CPs and tDNA reached 80 min while the maximal signal of tDNA and SPs appeared at 70 min, implying they were hybridized thoroughly with each other. Thus, 80 min and 70 min were selected as suitable incubation times for tDNA and SPs hybridization, respectively. The concentration of H_2O_2 was also optimized and the result is shown in Fig. S7E. The current response of this sensor increased along with the increasing concentration of H_2O_2 in the range of 2.5 - 15 mM. But the change of response signal was not obvious when over 15 mM, so we selected 15 mM of H_2O_2 in the experiment.

3.5. Analysis and detection

Under the optimized experiment conditions, the established sandwich-type electrochemical biosensor was used for the quantitative analysis of tDNA. The detection results can be seen in Fig. 4A, the current responses decreased gradually as the concentration of tDNA decreased. The fitted results (Fig. 4B) depicted a wide detection range from 10^{-8} mol/L to 10^{-16} mol/L with a low detection limit calculated to be 3.6×10^{-17} mol/L (S/N = 3) based on IUPAC definition [46,47]. The linear regression equation can be expressed as ΔCurrent (μA) = 5.94 lgC (mol/L) + 102.52 (R^2 = 0.994), where C represents the concentration of tDNA. The excellent analytic performance of the biosensor could be ascribed to the following factors. Firstly, the polyhedron structure of HAC provides a large surface to disperse AuPt alloy nanoparticles, resulting in preventing nanoparticles from aggregation and ensure more SPs could be fixed on the surface of nanocomposites. Moreover, the combination of both HAC and AuPt endows the resultant HAC-AuPt with multiple active sites including Co species, N species, graphitized carbon, and the synergistic or bifunctional effect of AuPt alloy nanoparticles, thus amplifying the signal. The results

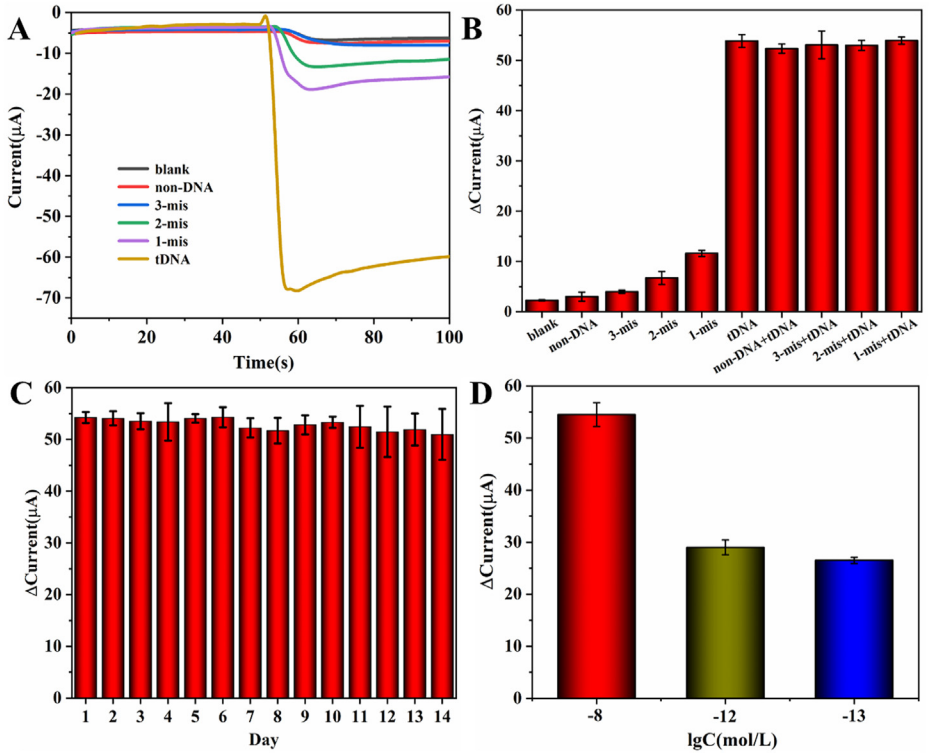

Fig. 5. Selectivity of the fabricated biosensor: **(A)** Amperometric responses of the biosensor towards different DNA sequences in pure samples and **(B)** The histogram of corresponding current responses in pure and mixed samples. **(C)** Stability and **(D)** Reproducibility investigation of the biosensor.

listed in Table S2 further highlight that the excellent performance of this biosensor makes it a promising method in ctDNA detection.

3.6. Selectivity, stability, and reproducibility

To assess the selectivity of this fabricated biosensor towards tDNA and other base-mismatched DNA sequences containing one base-mismatched (1-mis), two base-mismatched (2-mis), three base-mismatched (3-mis) DNA and non-complementary DNA (non-DNA), the current responses of the biosensor towards these DNA sequences (10^{-8} mol/L) were recorded under same conditions. The response of tDNA was larger than other interferences (Fig. 5A) and the signals of mixed DNA were almost the same as pure tDNA (Fig. 5B). The results illustrate the excellent selectivity of this proposed biosensor towards target DNA, especially its good identification ability for the single base-mutated sequence which is the most challenging recognition process in all base-mismatched DNA sequences. Also, the long-term stability of the biosensor was studied by recording the I-t signal variation of the modified electrodes within two weeks. The involved concentration of tDNA was 10^{-8} mol/L and the electrodes were stored in a refrigerator at 4 °C when not in use. As shown in Fig. 5C, a slight change of the current responses was observed after 14 days and it remained a signal of 93.9% compared with its original current, indicating the good stability of this biosensor. Last but not the least, the reproducibility of the biosensor was also investigated by using three groups (each group contained five individuals) of modified electrodes to detect tDNA with different concentrations (10^{-8} mol/L, 10^{-12} mol/L, 10^{-13} mol/L). The results (Fig. 5D) indicate that the recommended biosensor holds satisfying reproducibility with relative standard deviations (RSD) of 4.61%, 5.36%, and 2.42%.

3.7. Analysis of serum samples

To further evaluate the feasibility and credibility of the established biosensor in real sample analysis, a recovery experiment was carried out by a standard addition method. Specifically, tDNA with different concentrations (10^{-8} mol/L, 10^{-9} mol/L, 10^{-10} mol/L, 10^{-11} mol/L) were spiked into the ten-fold diluted serum of healthy humans. As listed in Table S3, the recovery rates were 94.8%, 92.6%, 98.4%, and 105.1% with acceptable RSD values of 1.61%, 4.73%, 4.00%, and 9.03%, respectively. The results confirm the good reliability of the biosensor for the detection of ctDNA in real samples.

4. Conclusions

In conclusion, a sensitive sandwich-type electrochemical biosensor based on HAC-AuPt nanocomposites was successfully developed for the detection of ctDNA. Through a facile calcination process and an in-situ reduction reaction, the synthesized HAC-AuPt contains multiple active sites for both improving the electrochemical property and bounding with SPs. After the hybridization of tDNA and SPs-label to form a sandwich structure, the H_2O_2 was added to PBS for triggering the current response. Thanks to the excellent catalytic capacity of the label HAC-AuPt, the current signal can be efficiently amplified. Consequently, the biosensor prepared in this study exhibits high sensitivity for the detection of tDNA and could distinguish other base-mismatched DNA sequences (even for the single base-mutated sequence). Furthermore, the proposed biosensor displays good long-term stability, reproducibility, and recovery rate, indicating a promising usage in clinical diagnosis in the future. This work offers a new method to synthesize labels of signal amplification for the improvement of biosensors' detection performance.

CRediT authorship contribution statement

Kaicha Chen: Methodology, Visualization, Validation, Writing – original draft, Writing – review & editing. **Hongli Zhao:** Project administration, Funding acquisition, Supervision, Methodology, Writing – review & editing. **Zhenxing Wang:** Methodology, Writing – review & editing. **Minbo Lan:** Project administration, Funding acquisition, Supervision, Methodology, Writing – review & editing.

Declaration of competing interest

The authors declare that they have no known competing financial interests or personal relationships that could have appeared to influence the work reported in this paper.

Acknowledgments

This work was supported by the Natural Science Foundation of Shanghai (19ZR1412000); the Science and Technology Commission of Shanghai Municipality (STCSM, 20520712500); the Fundamental Research Funds for the Central Universities (JKJ01211718); and the Predict Project (Shanghai University No.18SKY00, AUT FFG No. 870027). The authors thank the Research Center of Analysis and Test of East China University of Science and Technology for the help of X-ray photoelectron spectrometer analysis.

Appendix A. Supplementary data

Supplementary data to this article can be found online at https://doi.org/10.1016/j.aca.2021.338628.

References

[1] X.Y. Li, M.S. Ye, W.Y. Zhang, D. Tan, N. Jaffrezic-Renault, X. Yang, Z.Z. Guo, Liquid biopsy of circulating tumor DNA and biosensor applications, Biosens. Bioelectron. 126 (2019) 596–607.
[2] S.L. Hayward, P.E. Lund, Q. Kang, A. Johnson-Buck, M. Tewari, N.G. Walter, Ultraspecific and amplification-free quantification of mutant DNA by single-molecule kinetic fingerprinting, J. Am. Chem. Soc. 140 (2018) 11755–11762.
[3] J. Das, S.O. Kelley, High-performance nucleic acid sensors for liquid biopsy applications, Angew. Chem. Int. Ed. 59 (2020) 2554–2564.
[4] R. Vaidyanathan, R.H. Soon, P. Zhang, K. Jiang, C.T. Lim, Cancer diagnosis: from tumor to liquid biopsy and beyond, Lab Chip 19 (2018) 11–34.
[5] L. Gorgannezhad, M. Umer, M.N. Islam, N.T. Nguyen, M.J.A. Shiddiky, Circulating tumor DNA and liquid biopsy: opportunities, challenges, and recent advances in detection technologies, Lab Chip 18 (2018) 1174–1196.
[6] J. Das, I. Ivanov, E.H. Sargent, S.O. Kelley, DNA clutch probes for circulating tumor DNA analysis, J. Am. Chem. Soc. 138 (2016) 11009–11016.
[7] K. Gorges, L. Wiltfang, T.M. Gorges, A. Sartori, L. Hildebrandt, L. Keller, B. Volkmer, S. Peine, A. Babayan, I. Moll, S.W. Schneider, S. Twarock, P. Mohr, J.W. Fischer, K. Pantel, Intra-patient heterogeneity of circulating tumor cells and circulating tumor DNA in blood of melanoma patients, Cancers (2019) 11.
[8] M.R. Ossandon, L. Agrawal, E.J. Bernhard, B.A. Conley, S.M. Dey, R.L. Divi, P. Guan, T.G. Lively, T.C. McKee, B.S. Sorg, J.V. Tricoli, Circulating tumor DNA assays in clinical cancer research, J. Natl. Cancer Inst. 110 (2018) 929–934.
[9] F. Diehl, K. Schmidt, M.A. Choti, K. Romans, S. Goodman, M. Li, K. Thornton, N. Agrawal, L. Sokoll, S.A. Szabo, K.W. Kinzler, B. Vogelstein, L.A. Diaz Jr., Circulating mutant DNA to assess tumor dynamics, Nat. Med. 14 (2008) 985–990.
[10] J. Zhang, Y.H. Dong, W.F. Zhu, D. Xie, Y.L. Zhao, D.Y. Yang, M. Li, Ultrasensitive detection of circulating tumor DNA of lung cancer via an enzymatically amplified SERS-based frequency shift assay, ACS Appl. Mater. Interfaces 11 (2019) 18145–18152.
[11] Y.L. Chu, B. Cai, Y. Ma, M.G. Zhao, Z.Z. Ye, J.G. Huang, Highly sensitive electrochemical detection of circulating tumor DNA based on thin-layer MoS_2/graphene composites, RSC Adv. 6 (2016) 22673–22678.
[12] C.Y. Cai, Z.Z. Guo, Y.P. Cao, W.Y. Zhang, Y. Chen, A dual biomarker detection platform for quantitating circulating tumor DNA (ctDNA), Nanotheranostics 2 (2018) 12–20.
[13] H.F. Wang, R.N. Ma, F. Sun, L.P. Jia, W. Zhang, L. Shang, Q.W. Xue, W.L. Jia, H.S. Wang, A versatile label-free electrochemical biosensor for circulating tumor DNA based on dual enzyme assisted multiple amplification strategy, Biosens. Bioelectron. 122 (2018) 224–230.

[14] D.D. Li, Y.X. Xu, L. Fan, B. Shen, X.J. Ding, R. Yuan, X.M. Li, W.X. Chen, Target-driven rolling walker-based electrochemical biosensor for ultrasensitive detection of circulating tumor DNA using doxorubicin@tetrahedron-Au tags, Biosens. Bioelectron. 148 (2020), 111826.
[15] Y.H. Cheng, P.A.R. Moura, L. Zhenglong, L.X. Feng, S. Arokiam, J.L. Yang, M. Hariharan, S. Basuray, Effect of electrode configuration on the sensitivity of nucleic acid detection in a non-planar, flow-through, porous interdigitated electrode, Biomicrofluidics 13 (2019), 064118.
[16] Q. Yan, Y.Y. Yang, Z.L. Tan, Q. Liu, H. Liu, P. Wang, L. Chen, D.P. Zhang, Y.Y. Li, Y.H. Dong, A label-free electrochemical immunosensor based on the novel signal amplification system of AuPdCu ternary nanoparticles functionalized polymer nanospheres, Biosens. Bioelectron. 103 (2018) 151–157.
[17] Y.G. Wang, G.H. Zhao, H. Wang, W. Cao, B. Du, Q. Wei, Sandwich-type electrochemical immunoassay based on Co_3O_4@MnO_2-thionine and pseudo-ELISA method toward sensitive detection of alpha fetoprotein, Biosens. Bioelectron. 106 (2018) 179–185.
[18] X.L. Jia, X. Chen, J.G. Han, J. Ma, Z. F Ma, Triple signal amplification using gold nanoparticles, bienzyme and platinum nanoparticles functionalized graphene as enhancers for simultaneous multiple electrochemical immunoassay, Biosens. Bioelectron. 53 (2014) 65–70.
[19] X.B. Zhang, Y.Y. Li, H. Lv, J.H. Feng, Z.Q. Gao, P. Wang, Y.H. Dong, Q. Liu, Z.D. Zhao, Sandwich-type electrochemical immunosensor based on Au@Ag supported on functionalized phenolic resin microporous carbon spheres for ultrasensitive analysis of alpha-fetoprotein, Biosens. Bioelectron. 106 (2018) 142–148.
[20] Y.K. Ye, S. Mao, S.D. He, X. Xu, X.D. Cao, Z.J. Wei, S. Gunasekaran, Ultrasensitive electrochemical genosensor for detection of CaMV35S gene with Fe_3O_4-Au@Ag nanoprobe, Talanta 206 (2020), 120205.
[21] X. Zhu, T.T. Liu, H.L. Zhao, L.B. Shi, X.Q. Li, M. B Lan, Ultrasensitive detection of superoxide anion released from living cells using a porous Pt–Pd decorated enzymatic sensor, Biosens. Bioelectron. 79 (2016) 449–456.
[22] Y. Li, J.L. He, J. Chen, Y.Z. Niu, Y.L. Zhao, Y.C. Zhang, C. Yu, A dual-type responsive electrochemical immunosensor for quantitative detection of PCSK9 based on n-C60-PdPt/N-GNRs and Pt-poly (methylene blue) nanocomposites, Biosens. Bioelectron. 101 (2018) 7–13.
[23] M.H. Lin, J.J. Wang, G.B. Zhou, J.B. Wang, N. Wu, J.X. Lu, J.M. Gao, X.Q. Chen, J.Y. Shi, X.L. Zuo, C.H. Fan, Programmable engineering of a biosensing interface with tetrahedral DNA nanostructures for ultrasensitive DNA detection, Angew. Chem. Int. Ed. 54 (2015) 2151–2155.
[24] Z.L. Tan, H. Dong, Q. Liu, H. Liu, P.P. Zhao, P. Wang, Y.Y. Li, D.P. Zhang, Z.D. Zhao, Y.H. Dong, A label-free immunosensor based on PtPd NCs@MoS_2 nanoenzymes for hepatitis B surface antigen detection, Biosens. Bioelectron. 142 (2019), 111556.
[25] L.Y. Wang, J. Shan, F. Feng, Z.F. Ma, Novel redox species polyaniline derivative-Au/Pt as sensing platform for label-free electrochemical immunoassay of carbohydrate antigen 199, Anal. Chim. Acta 911 (2016) 108–113.
[26] X. Zhu, X.H. Niu, H.L. Zhao, J. Tang, M.B. Lan, Immobilization of superoxide dismutase on Pt-Pd/MWCNTs hybrid modified electrode surface for superoxide anion detection, Biosens. Bioelectron. 67 (2015) 79–85.
[27] H. Lv, Y.Y. Li, X.B. Zhang, Z.Q. Gao, C.Y. Zhang, S. Zhang, Y.H. Dong, Enhanced peroxidase-like properties of Au@Pt DNs/NG/Cu(2+) and application of sandwich-type electrochemical immunosensor for highly sensitive detection of CEA, Biosens. Bioelectron. 112 (2018) 1–7.
[28] S.H. Baek, J. Roh, C.Y. Park, M.W. Kim, R. Shi, S.K. Kailasa, T.J. Park, Cu-nanoflower decorated gold nanoparticles-graphene oxide nanofiber as electrochemical biosensor for glucose detection, Mater. Sci. Eng. C Mater. Biol. Appl. 107 (2020), 110273.
[29] Y.Z. Chen, C. Wang, Z.Y. Wu, Y. Xiong, Q. Xu, S.H. Yu, H.L. Jiang, From bimetallic metal-organic framework to porous carbon: high surface area and multicomponent active dopants for excellent electrocatalysis, Adv. Mater. 27 (2015) 5010–5016.
[30] Y.F. Li, L.B. Shi, X. Cai, H.L. Zhao, X.H. Niu, M.B. Lan, Construction of non-enzymatic sensor based on porous carbon matrix loaded with Pt and Co nanoparticles for real-time monitoring of cellular superoxide anions, Electrochim. Acta 294 (2019) 304–311.
[31] Z. Wang, T.T. Yan, J.H. Fang, L.Y. Shi, D.S. Zhang, Nitrogen-doped porous carbon derived from a bimetallic metal-organic framework as highly efficient electrodes for flow-through deionization capacitors, J. Mater. Chem. A 4 (2016) 10858–10868.
[32] W.J. Shao, C. He, M. Zhou, C.D. Yang, Y. Gao, S. Li, L. Ma, L. Qiu, C. Cheng, C.S. Zhao, Core–shell-structured MOF-derived 2D hierarchical nanocatalysts with enhanced Fenton-like activities, J. Mater. Chem. A 8 (2020) 3168–3179.
[33] Y. Chen, Y. Li, D.G. Deng, H.B. He, X.X. Yan, Z.X. Wang, C.H. Fan, L.Q. Luo, Effective immobilization of Au nanoparticles on TiO_2 loaded graphene for a novel sandwich-type immunosensor, Biosens. Bioelectron. 102 (2018) 301–306.
[34] H. Jiang, E.M. Materon, M.D.P.T. Sotomayor, J. Liu, Fast assembly of non-thiolated DNA on gold surface at lower pH, J. Colloid Interface Sci. 411 (2013) 92–97.
[35] N. Dimitratos, A. Villa, D. Wang, F. Porta, D. Su, L. Prati, Pd and Pt catalysts modified by alloying with Au in the selective oxidation of alcohols, J. Catal. 244 (2006) 113–121.
[36] H.X. Ren, X.J. Huang, J.H. Kim, Y.K. Choi, N. Gu, Pt/Au bimetallic hierarchical structure with micro/nano-array via photolithography and electrochemical synthesis: from design to GOT and GPT biosensors, Talanta 78 (2009) 1371–1377.
[37] L. Jiao, Z.G. Mu, C.Z. Zhu, Q. Wei, H. Li, D. Du, Y.H. Lin, Graphene loaded bimetallic Au@Pt nanodendrites enhancing ultrasensitive electrochemical immunoassay of AFP, Sensor. Actuator. B Chem. 231 (2016) 513–519.
[38] I.A. Khan, M. Sofian, A. Badshah, M.A. Khan, M. Imran, M.A. Nadeem, Stable and efficient PtRu electrocatalysts supported on Zn-BTC MOF derived microporous carbon for formic acid fuel cells application, Front. Chem. 8 (2020) 367.
[39] X.Y. Fu, C.Z. Wan, A.X. Zhang, Z.P. Zhao, H.X. Huyan, X.Q. Pan, S.J. Du, X.F. Duan, Y. Huang, Pt_3Ag alloy wavy nanowires as highly effective electrocatalysts for ethanol oxidation reaction, Nano Res. 13 (2020) 1472–1478.
[40] J.M. Gu, W.S. Kim, Y.K. Hwang, S. Huh, Template-free synthesis of N-doped porous carbons and their gas sorption properties, Carbon 56 (2013) 208–217.
[41] L.J. Lu, Y. Nie, Y. Wang, G.G. Wu, L.J. Li, J. Li, X.Q. Qi, Z.D. Wei, Preparation of highly dispersed carbon-supported AuPt nanoparticles via a capping agent-free route for efficient methanol oxidation, J. Mater. Chem. A 6 (2018) 104–109.
[42] P. Gilad, T.V. Ran, E. Johann, W. Itamar, Amplified biosensing using the horseradish peroxidase-mimicking DNAzyme as an electrocatalyst, Anal. Chem. 82 (2010) 4396–4402.
[43] H.W. Wei, T.Y. Shang, T.D. Wu, G.A. Liu, L. Ding, X.H. Liu, Construction of an ultrasensitive non-enzymatic sensor to investigate the dynamic process of superoxide anion release from living cells, Biosens. Bioelectron. 100 (2018) 8.
[44] W. Zhang, Z.C. Dai, X. Liu, J.M. Yang, High-performance electrochemical sensing of circulating tumor DNA in peripheral blood based on polyxanthurenic acid-functionalized MoS_2 nanosheets, Biosens. Bioelectron. 105 (2018) 116.
[45] J. Sap, A. Muñoz, K. Damm, Y. Goldberg, J. Ghysdael, A. Leutz, H. Beug, B. Vennström, The c-erb-A protein is a high-affinity receptor for thyroid hormone, Nature 324 (1986) 635–640.
[46] X.L. Zhang, Z.H. Yang, Y.Y. Chang, D. Liu, Y.R. Li, Y.Q. Chai, Y. Zhuo, R. Yuan, Programmable mismatch-fueled high-efficiency DNA signal converter, Chem. Sci. 11 (2020) 148–153.
[47] A.E. Radi, J.L. Acero Sánchez, E. Baldrich, C.K. O'Sullivan, Reagentless, reusable, ultrasensitive electrochemical molecular beacon aptasensor, J. Am. Chem. Soc. 128 (2006) 117–124.